Video Article

Microparticle Manipulation by Standing Surface Acoustic Waves with Dual-frequency Excitations

Yufeng Zhou[1], Yannapol Sriphutkiat[1]

[1]School of Mechanical and Aerospace Engineering, Nanyang Technological University

Correspondence to: Yufeng Zhou at yfzhou@ntu.edu.sg

URL: https://www.jove.com/video/58085
DOI: doi:10.3791/58085

Keywords: Engineering, Issue 138, Microparticle manipulation, standing surface acoustic wave, dual-frequency excitation, power ratio, phase difference, microfluidic channel

Date Published: 8/21/2018

Citation: Zhou, Y., Sriphutkiat, Y. Microparticle Manipulation by Standing Surface Acoustic Waves with Dual-frequency Excitations. *J. Vis. Exp.* (138), e58085, doi:10.3791/58085 (2018).

Abstract

We demonstrate a method for increasing the tuning ability of a standing surface acoustic wave (SSAW) for microparticles manipulation in a lab-on-a-chip (LOC) system. The simultaneous excitation of the fundamental frequency and its third harmonic, which is termed as dual-frequency excitation, to a pair of interdigital transducers (IDTs) could generate a new type of standing acoustic waves in a microfluidic channel. Varying the power and the phase in the dual-frequency excitation signals results in a reconfigurable field of the acoustic radiation force applied to the microparticles across the microchannel (*e.g.*, the number and location of the pressure nodes and the microparticle concentrations at the corresponding pressure nodes). This article demonstrates that the motion time of the microparticle to only one pressure node can be reduced ~2-fold at the power ratio of the fundamental frequency greater than ~90%. In contrast, there are three pressure nodes in the microchannel if less than this threshold. Furthermore, adjusting the initial phase between the fundamental frequency and the third harmonic results in different motion rates of the three SSAW pressure nodes, as well as in the percentage of microparticles at each pressure node in the microchannel. There is a good agreement between the experimental observation and the numerical predictions. This novel excitation method can easily and non-invasively integrate into the LOC system, with a wide tenability and only a few changes to the experimental set-up.

Video Link

The video component of this article can be found at https://www.jove.com/video/58085/

Introduction

LOC technology integrates one or several functions on a microchip for biology, chemistry, biophysics, and biomedical processes. LOC allows a laboratory set-up on a scale smaller than sub-millimeters, fast reaction rates, a short response time, a high process control, a low volume consumption (less waste, lower reagents cost, and less required sample volume), a high throughput due to parallelization, a low cost in the future mass production and cost-effective disposables, a high safety for chemical, radioactive, or biological studies, and the advantages of a compact and portable device[1,2]. Precise cell manipulation (*i.e.*, accumulation and separation) is critical in an LOC-based analysis and diagnosis[3,4]. However, the accuracy and reproducibility of microparticle manipulation have a variety of challenges. Many techniques, such as electro-osmosis[5], dielectrophoresis (DEP)[6], magnetophoresis[7], thermophoresis[8,9], an optical approach[10], an optoelectronic approach[11], a hydrodynamic approach[12], and acoustophoresis[13,14,15], have been developed. In comparison, acoustic approaches are appropriate for a LOC application because, theoretically, many types of microparticles/cells can be manipulated effectively and noninvasively with a sufficiently high contrast (density and compressibility) compared with the surrounding fluid. Therefore, compared to their counterparts, acoustic approaches are inherently eligible for most microparticles and biological objects, no matter their optical, electrical, and magnetic properties[16].

Surface acoustic waves (SAWs) from the IDTs propagate mostly on the surface of a piezoelectric substrate at the thickness of several wavelengths and then leak at the Rayleigh angle into the fluid in the microchannel, according to the Snell's law[17,18,19,20,21,22]. They have the technical advantages of a high energy efficiency along the surface due to their localization of the energy, a great design flexibility at high frequency, a good system integration with the microfluidic channel and miniaturization using micro-electronic-mechanical system (MEMS) technology, and a high potential of mass production[23]. In this protocol, SAWs are generated from a pair of identical IDTs and propagated in the opposite direction to generate a standing wave, or SSAW, in the microchannel, where the suspended microparticles are pushed to pressure nodes, mostly by the applied acoustic radiation force[24]. The amplitude of such resultant force is determined by the excitation frequency, microparticle size, and its acoustic contrast factor[22,25].

Such acoustophoresis has the limitation of predetermined manipulating patterns that are not easily adjustable. The excitation frequency of the IDTs is determined by their periodic distance, so the bandwidth is quite limited. Several strategies have been developed to enhance the tunability and manipulation capability. The first and second modes of acoustic standing waves applied in different parts of the microchannel could separate microparticles more effectively according to different motion speeds toward the nodal lines[26]. These two modes could also be applied to the whole part of the microchannel and switched alternatively[27,28,29]. However, for this, a large number of equipment (*i.e.*, three function generators, two impedance matching units, and an electromagnetic relay) is required, with the increased cost and control complexity of the experimental

set-up owing to the different electrical impedances at the fundamental frequency and third harmonic of the piezoceramic plate[30]. Furthermore, slanted-finger interdigital transducers (SFITs) could be applied to adjust the cells and the microparticles patterning by exciting a period of the slanted fingers for a certain resonance[20,31]. However, then, the bandwidth is inversely proportional to the number of slanted fingers. Multiple pressure nodal lines have a higher separation efficiency and sensitivity in comparison to the single nodal line in the conventional SSAW-based microparticle separator. Alternatively, the location of the pressure nodes could also be changed simply by adjusting the phase difference applied to the two IDTs in the design[32,33].

The fundamental frequency and the third harmonic of IDTs have similar frequency responses so that they can be excited simultaneously, which provides more tunability for the microparticles manipulation[34]. In comparison to the conventional IDT excitation at a single frequency, adjusting the acoustic pressures of the dual-frequency excitation and the phase between them provides technical uniqueness, such as the up to ~2-fold reduced motion time to the pressure nodal line or the center of the microchannel, the varied number and location of the pressure nodal lines, and the microparticle concentrations.

Protocol

1. Preparation of the Microfluidic Channel

1. Mix poly-dimethylsiloxane (PDMS) with an elastomer base in a ratio of 10:1.
2. Degas the mixture in a vacuum oven and pour it on a silicon wafer with a negative tone photoresist pattern on the top.
3. Degas the patterned silicon wafer again and heat it at 70 °C for 3 h in an incubator for solidification.

2. Fabrication of the Interdigital Transducers

1. Deposit 20 nm of Cr and 400 nm of Al on a $LiNbO_3$ wafer; pattern 20 strips with a width of 150 µm and an aperture of 2 cm on a plastic mask for photolithography by depositing the positive photoresist on the substrate.
2. Remove the Cr-Al layer on the non-exposed area with acetone.
3. Treat the surface of them with oxygen plasma (with a nitrogen and oxygen ratio of 2:1) at the power of 30 W for 60 s.
4. Align the PDMS microchannel and bond it to the $LiNbO_3$ substrate by pressing it with a thumb for a few seconds.
5. Place the integrated device in the heating chamber at 60 °C for 3 h.

3. Dual-frequency Excitation

1. Simultaneously apply two frequency components (f_1 and f_3, the fundamental frequency and its third harmonic of the fabricated IDT, respectively) with the phase difference φ between them to the pair of IDTs, so that the produced SAW may be expressed as follows.
$$p(t) = p_1 \sin(2\pi f_1 t) + p_3 \sin(2\pi f_3 t + \varphi)$$
Here,
p_1 and p_3 = the acoustic pressures.
2. Synthesize the dual-frequency waveform using the **Equation Editor** of the ArbExpress Application software at the sampling frequency of 100 MS/s and then store it to the function generator as arbitrary input for the SAW excitation in the experiment *via* a USB cable.
3. Vary the power of the fundamental frequency to the total emitted power $P_1 = \frac{p_1^2}{p_1^2+p_3^2}$ from 100% (excitation at the purely fundamental frequency) to 0% (excitation at the purely third harmonic); for a good comparison, change but keep the total power the same.
4. Vary the phase difference of the dual-frequency excitation from 0° to 360°.

4. Numerical Simulation

1. Describe the motion of the incompressible laminar flow with low Reynolds (*i.e.*, *Re* = 0.55) and Mach numbers as follows[35].
$$\rho_0(\vec{u}\cdot\nabla)\vec{u} = \nabla\cdot\left[-p\cdot\boldsymbol{I} + \mu(\nabla\vec{u} + (\nabla\vec{u})^T)\right] + \vec{F}$$
$$\rho_0\nabla\cdot(\vec{u}) = 0$$
Here,
$\vec{u}$ = the fluid velocity,
μ = the dynamic viscosity,
ρ_0 = the fluid density,
p = the pressure on the fluid,
$\boldsymbol{I}$ = the identity matrix, and
$\vec{F}$ = an external force.
2. Describe the produced Stoke drag force on the object as follows[36].
$$F_D = 6\pi\mu r\,(v_{fluid} - v_{particle})$$
Here,
r = the radius of the microparticle,
v_{fluid} = the velocity of the fluid, and
$v_{particle}$ = the velocity of the microparticle.

3. Derive the acoustic radiation force applied to the microparticle in the microchannel along the *x*-axis (across the microchannel width) at a single frequency as follows[16] .

$$F_{rad} = -\left(2kp_0^2 V_p \beta_m\right)\left(\frac{5\rho_p - 2\rho_m}{2\rho_p + \rho_m} - \frac{\beta_p}{\beta_m}\right)\sin(2kx) \quad = Akp_0^2 \sin(2kx)$$

Here,
V_p = the volume of the microparticle,
ρ_p = the density of the microparticle,
ρ_m = the density of the medium,
β_p = the compressibility of the microparticle, and
β_m = the compressibility of the medium.

4. Derive the resultant acoustic radiation force of the dual-frequency excitation as follows.

$$F'_{rad} + F''_{rad} = A[k_1 p_1^2 \sin(2k_1 x) + k_3 p_3^2 \sin(2k_3 x + 2\varphi)]$$

5. Express the transverse motion across the channel width (along the *y*-axis) under both the acoustic radiation force and the Stokes drag force governed by Newton's second law as follows.

$$m\frac{d^2 y}{dt^2} = F_r(y,t) + F_D(y,t)$$

6. Solve the ordinary differential equations (ODEs) above using the fourth order Runge-Kutta method on a personal computer.Set the time step and total duration as 1 μs and 20 s, respectively.

5. Experimental Observation

1. Spin the solution in the concentration of 5.9 x 10^7 with 4 μm green fluorescent polystyrene beads per 1 mL by vortex for about 2 - 3 min and then immerse it in an ultrasound sonicator for 10 min to disrupt any agglomeration before each testing.
2. Fill the mixture into a 3 mL syringe and then drive it with a syringe pump at a flow rate of 3 - 5 μL/min.
3. Drive the IDT with the dual-frequency signal from a function generator followed by a power amplifier.
4. Observe the stabilized microparticles in the downstream microchannel under a light microscope at a 40X magnification and record the image with a digital camera.
5. Measure the location of the accumulated microparticles in the captured digital images using ImageJ and the established scale, and then quantitatively determine the concentration of the accumulated microparticle with the normalized fluorescence brightness at each pressure node.

Representative Results

The distributions of the acoustic pressure and the acoustic radiation force of an SSAW at the dual-frequency excitation (6.2 and 18.6 MHz) are shown in **Figure 1**. Here, the dual-frequency excitation occurs on polystyrene microparticles (4 μm in diameter) in a microchannel with a width of 300 μm at an acoustic power of 146 mW. The resultant acoustic pressure is always in phase when P_1 > 90% so that only one pressure node is present at *y* = 150 μm. In contrast, three pressure nodes are present at *y* = 75, 150, and 225 μm at P_1 = 90%, and at *y* = 50, 150, and 250 μm at P_1 = 0%. The threshold of P_1 = 90% is found almost constant throughout all testing conditions, as is a microparticle diameter of 4 - 10 μm, a total acoustic power of 73 - 648 mW, and a driving frequency of 6.2 - 18.6 MHz.

At P_1 = 90%, the microparticles in the region of 75 μm < *y* < 255 μm and 0 μm ≤ *y* ≤ 75 μm move toward the central and the lower pressure node, respectively. In comparison, at P_1 = 0%, the regions for the central and the lower pressure nodes are changed to 100 μm < *y* < 200 μm and 0 μm ≤ *y* ≤ 100 μm, respectively. Subsequently, the microparticle concentrations at the lower node vary from 25% to 33.3%, and at central nodes from 50% to 33.3%, when decreasing P_1 from 90% to 0%, respectively (see **Figure 2a**). The motion time of the microparticle toward the pressure node is reduced from about 1.95 s at P_1 = 100% to 0.97 s at P_1 = 95% (see **Figure 2b**). The dependence of the position of the pressure node and the microparticle concentration on P_1, measured experimentally, has a good correlation with the numerical prediction (R^2 = 0.85 in **Figure 2c** and R^2 = 0.83 in **Figure 2d**). A large number of power ratios were tested (*n* > 31), and the variations in the position of accumulated microparticles (6.8 - 10.6%) are much smaller than those in the particle concentration at the pressure nodes (6.7 - 31.4%), which may be due to the occurrence of agglomeration during the microparticle accumulation.

The initial phase of the third harmonic in the dual-frequency excitation affects the synthesized driving waveform, the resultant acoustic radiation force to the microparticle, and the location of the pressure node (see **Figure 3**). With an increase of φ from 0° to 180°, the three pressure nodes (*y* = 63.5, 150, and 236.5 μm) will gradually shift downward across the microchannel. As P_1 was fixed at 85%, the lower pressure node is located at *y* = 49.5 μm, 33.5 μm, 17 μm, and 0 μm and at φ = 45°, 90°, 135°, and 180°, respectively. The acoustic radiation forces from f_1 and f_3 are out of phase at φ = 0°, while in phase at φ = 180°. For example, at *y* = 75 μm and φ = 0°, the maximum acoustic radiation forces of f_1 and f_3 are 37.68 pN and -47.49 pN, respectively. While at φ = 180°, the maximum acoustic radiation force from f_1 and f_3 at the same position are 37.68 pN and 47.49pN, respectively. All pressure nodes shift downward across the microchannel in a linear manner with the increase of φ. It is noted that the lower pressure node shifts at a much faster rate than those of the center and the upper pressure nodes (*i.e.*, from 63.5 to 0 μm, from 150 to 110.6 μm, and from 236.5 μm to 190.1 μm with the change of φ from 0° to 180°). At φ = 180°, there are 4 pressure nodes. After that, the pressure node at the lower boundary (*y* = 0 μm) disappears, and that at the upper boundary (*y* = 300 μm) shifts downward at the same rate as the lower pressure node with the change of φ from 0° to 180°. At φ = 360°, the pressure node replaces an adjacent one (*i.e.*, the upper pressure node at φ = 360° has the same location as the central pressure node at φ = 0°). The experimental results have a good agreement with the numerical prediction, especially those of the location of the pressure node at different phases.

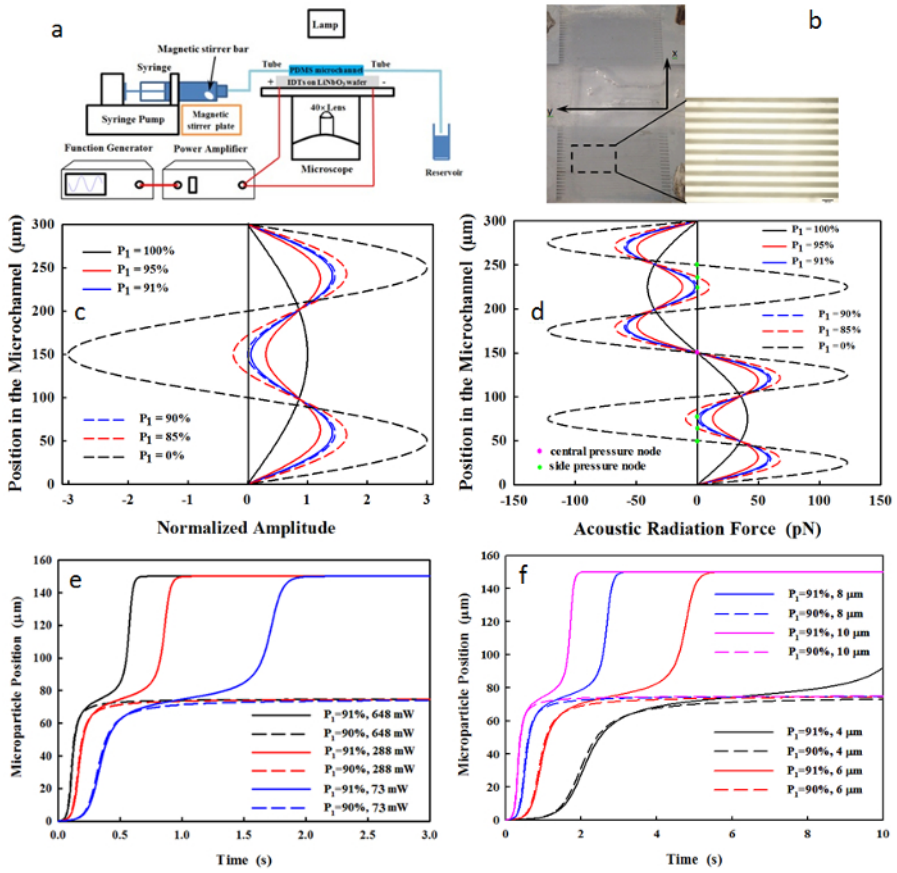

Figure 1. (a) Schematic diagram of experimental setup and (b) photo of IDTs and PDMS microchannel (scale of 300 μm). (c) The pressure waveform and (d) the corresponding acoustic radiation force applied to the 4-μm microspheres in a 300-μm microfluidic channel by the dual-frequency excitation at the varied power ratios of P1 = 100% (purely fundamental frequency), 95%, 91%, 90%, 85%, and 0% (purely third harmonic) at the total acoustic power of 146 mW. Motion of microparticle initially at y = 0 μm (e) with the diameter of 4 μm under the varied power ratios (88-91%) and total acoustic powers (73-648 mW) and (f) with the varied diameters of 4, 6, 8, and 10 μm at the total acoustic power of 73 mW. This figure has been modified from Sriphutkiat, Y., *et al.*[34]. Please click here to view a larger version of this figure.

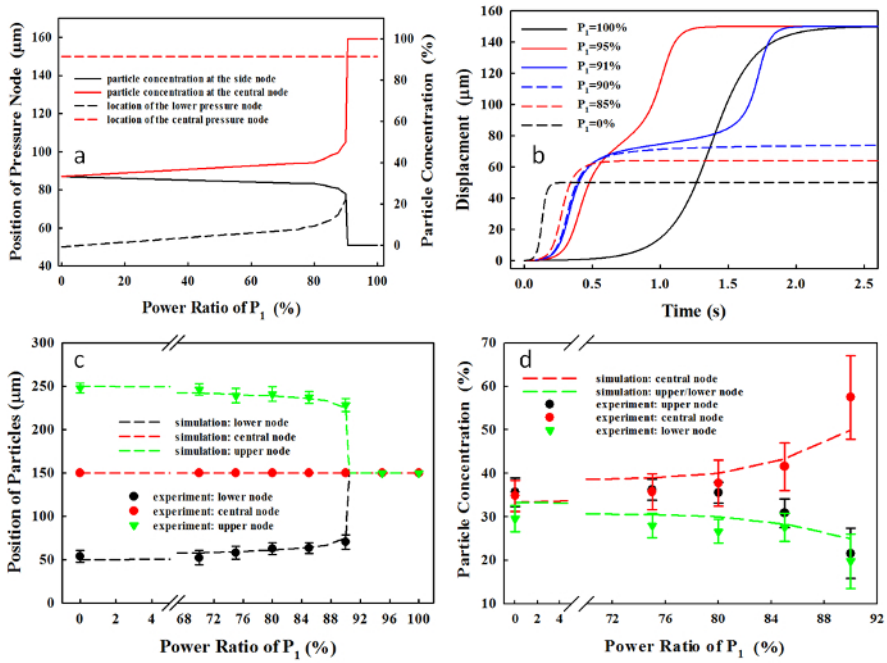

Figure 2. (a) Microparticle position and concentration, (b) motion of microparticles initially at y_0 = 0 μm, and the microparticle accumulation time using the dual-frequency excitation at the total acoustic power of 146 mW with varied power ratios. Comparison of the simulation and experimental results (mean standard deviation) of (c) the position of pressure node (R^2 = 0.85, n = 37) and (d) the microparticle concentration at each pressure node in the microchannel (R^2 = 0.83, n = 31) at the varied power ratios of P_1. This figure has been modified from Sriphutkiat, Y., *et al.*[34]. Please click here to view a larger version of this figure.

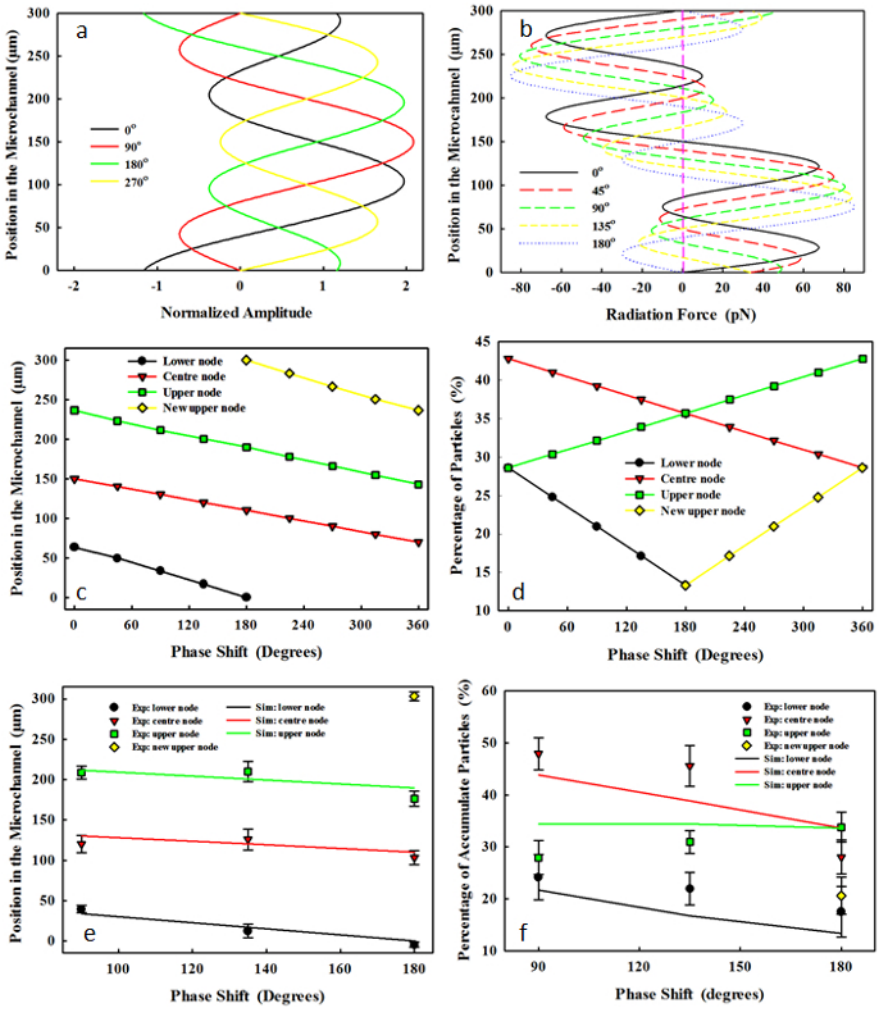

Figure 3. (a) The synthesized waveform at the dual-frequency excitation, (b) the distribution of resultant acoustic radiation force across the 300-μm microchannel at the varied initial phase from 0° to 180° at the power ratio of 85%. The effects of the initial phase at the dual-frequency excitation, Ø, on the location of pressure node in the (c) simulation and (e) experiment (mean ± standard deviation) and the percentage of microparticles accumulated at each pressure node in the (d) simulation and (f) experiment. Please click here to view a larger version of this figure.

Discussion

The microparticle motion in the microchannel by an SSAW at the dual-frequency excitation was extensively investigated in this study, and an effectively tunable patterning technique by varying the dual-frequency excitation signals was developed and tested. The production of such a waveform is easily realized by most function generators, and the adjusting approach is very convenient. Both the S_{12}- and S_{11}-frequency responses of the fabricated IDTs illustrate several resonant modes[34]. The measured fundamental frequency of 6.1 MHz and the third harmonic of 17.8 MHz are close to those designed values (6.2 and 18.6 MHz) with similar transmission coefficients, -8.34 dB *vs.* -9.75 dB, respectively. Thus, a similar acoustic energy output at these two components at the dual-frequency excitation using the single IDT is expected. Such a component combination is not only limited to f_1 and f_3. Others, such as f_1 and f_5, and f_3 and f_5, are also applicable. Although piezoceramics can also generate different harmonics of the bulk acoustic, simultaneous excitation of them is impossible. Switching the acoustic field could enhance the microparticle sorting[29] but at the cost of more equipment and a high control complexity.

The number and location of pressure nodes in the microchannel and the corresponding microparticle concentrations could be tuned conveniently and effectively by the dual-frequency excitation without changing other parts. Only one pressure node at $P_1 > 90\%$ is the same as that produced by the fundamental frequency. However, there are three pressure nodes with varied positions and a microparticle concentration below this threshold. This threshold is found constant for all testing parameters here, such as the driving frequency, the acoustic power, and the diameter of microparticles. The experimental results correlate quite well with the theoretical prediction. By using this proposed strategy, the motion time of microparticles could be reduced up to ~2-fold, which suggests a higher throughput.

Phase modulation with dual frequency provides a flexible control of the pressure nodes location. Shifting other pressure nodes away or adjusting the direction of the acoustic radiation force inward may be a simple way to increase the number of the microparticles on the specific pressure node. At $\varphi \geq 180°$, the pressure node at the bottom of the microchannel will disappear, but the one at the top will show up. At φ =

360°, the replacement of pressure nodes occurs. Thus, pressure nodal lines continuously move with the varied phase between two frequency components.

In this study, there are still some limitations. More acoustic attenuation and viscous heating of the wall material may be introduced when a SAW propagates through a thick PDMS microchannel[37]. Parasitic wave excitation in the wall, such as from a bulk acoustic wave, may also actuate the fluid in the microchannel. Experiments using the biological cells are in a great need for clinical use.

This acoustical LOC is inherently non-invasive, and this new excitation strategy could enhance the tenability and manipulation, which has great potential in many applications. Dual-frequency excitation in biological diagnoses, such as isolating circulating tumor cells (CTCs), may provide information about the occurrence of metastasis and, subsequently, request immediate treatment.

Disclosures

The authors have nothing to disclose.

Acknowledgements

This work was sponsored by the Academic Research Fund (AcRF) Tier 1 (RG171/15), Ministry of Education, Singapore.

References

1. Chin, C. D., Linder, V., Sia, S. K. Commercialization of microfluidic point-of-care diagnostic devices. *Lab on a Chip.* **12** (12), 2118-2134 (2012).
2. Figeys, D., Pinto, D. Lab-on-a-chip: a revolution in biological and medical sciences. *Analytical Chemistry.* **72** (9), 330 A-335 A (2000).
3. den Toonder, J. Circulating tumor cells: the Grand Challenge. *Lab on a Chip.* **11** (3), 375-377 (2011).
4. Yu, L. *et al.* Advances of lab-on-a-chip in isolation, detection and post-processing of circulating tumour cells. *Lab on a Chip.* **13** (16), 3163-3182 (2013).
5. Jorgenson, J. W., Lukacs, K. D. High-resolution separations based on electrophoresis and electroosmosis. *Journal of Chromatography A.* **218**, 209-216 (1981).
6. Gascoyne, P. R., Vykoukal, J. Particle separation by dielectrophoresis. *Electrophoresis.* **23** (13), 1973 (2002).
7. Xia, N. *et al.* Combined microfluidic-micromagnetic separation of living cells in continuous flow. *Biomedical Microdevices.* **8** (4), 299-308 (2006).
8. Garcés-Chávez, V. *et al.* Extended organization of colloidal microparticles by surface plasmon polariton excitation. *Physical Review B.* **73** (8), 085417 (2006).
9. Zhu, T., Ye, W. Origin of Knudsen forces on heated microbeams. *Physical Review E.* **82** (3), 036308 (2010).
10. Ashkin, A., Dziedzic, J., Yamane, T. Optical trapping and manipulation of single cells using infrared laser beams. *Nature.* **330** (6150), 769-771 (1987).
11. Chiou, P. Y., Ohta, A. T., Wu, M. C. Massively parallel manipulation of single cells and microparticles using optical images. *Nature.* **436** (7049), 370-372 (2005).
12. Yamada, M., Seki, M. Hydrodynamic filtration for on-chip particle concentration and classification utilizing microfluidics. *Lab on a Chip.* **5** (11), 1233-1239 (2005).
13. Burguillos, M. A. *et al.* Microchannel acoustophoresis does not impact survival or function of microglia, leukocytes or tumor cells. *PLoS One.* **8** (5), e64233 (2013).
14. Lin, S.-C. S., Mao, X., Huang, T. J. Surface acoustic wave (SAW) acoustophoresis: now and beyond. *Lab on a Chip.* **12** (16), 2766-2770 (2012).
15. Petersson, F., Åberg, L., Swärd-Nilsson, A.-M., Laurell, T. Free flow acoustophoresis: microfluidic-based mode of particle and cell separation. *Analytical Chemistry.* **79** (14), 5117-5123 (2007).
16. Ding, X. *et al.* On-chip manipulation of single microparticles, cells, and organisms using surface acoustic waves. *Proceedings of the National Academy of Sciences.* **109** (28), 11105-11109 (2012).
17. Friend, J., Yeo, L. Y. Microscale acoustofluidics: Microfluidics driven via acoustics and ultrasonics. *Reviews of Modern Physics.* **83** (2), 647 (2011).
18. Destgeer, G., Lee, K. H., Jung, J. H., Alazzam, A., Sung, H. J. Continuous separation of particles in a PDMS microfluidic channel via travelling surface acoustic waves (TSAW). *Lab on a Chip.* **13** (21), 4210-4216 (2013).
19. Guo, F. *et al.* Controlling cell-cell interactions using surface acoustic waves. *Proceedings of the National Academy of Sciences.* **112** (1), 43-48 (2015).
20. Ding, X. *et al.* Cell separation using tilted-angle standing surface acoustic waves. *Proceedings of the National Academy of Sciences.* **111** (36), 12992-12997 (2014).
21. Roshchupkin, D. *et al.* X-ray diffraction by standing surface acoustic waves. *Nuclear Instruments and Methods in Physics Research Section B: Beam Interactions with Materials and Atoms.* **142** (3), 432-436 (1998).
22. Shi, J., Mao, X., Ahmed, D., Colletti, A., Huang, T. J. Focusing microparticles in a microfluidic channel with standing surface acoustic waves (SSAW). *Lab on a Chip.* **8** (2), 221-223 (2008).
23. Ding, X. *et al.* Surface acoustic wave microfluidics. *Lab on a Chip.* **13** (18), 3626-3649 (2013).
24. King, L. V. in *Proceedings of the Royal Society of London A: Mathematical, Physical and Engineering Sciences.* 212-240. The Royal Society. (1934).
25. Yosioka, K., Kawasima, Y. Acoustic radiation pressure on a compressible sphere. *Acta Acustica United with Acustica.* **5** (3), 167-173 (1955).
26. Ratier, C., Hoyos, M. Acoustic programming in step-split-flow lateral-transport thin fractionation. *Analytical Chemistry.* **82** (4), 1318-1325 (2010).

27. Mandralis, Z., Feke, D., Bolek, W., Burger, W., Benes, E. Enhanced synchronized ultrasonic and flow-field fractionation of suspensions. *Ultrasonics.* **32** (2), 113-122 (1994).
28. Laurell, T., Petersson, F., Nilsson, A. Chip integrated strategies for acoustic separation and manipulation of cells and particles. *Chemical Society Reviews.* **36** (3), 492-506 (2007).
29. Liu, Y., Lim, K.-M. Particle separation in microfluidics using a switching ultrasonic field. *Lab on a Chip.* **11** (18), 3167-3173 (2011).
30. Brissaud, M. Characterization of piezoceramics. *IEEE Transactions on Ultrasonics, Ferroelectrics, and Frequency Control.* **38** (6), 603-617 (1991).
31. Ding, X. *et al.* Tunable patterning of microparticles and cells using standing surface acoustic waves. *Lab on a Chip.* **12** (14), 2491-2497 (2012).
32. Jo, M. C., Guldiken, R. Particle manipulation by phase-shifting of surface acoustic waves. *Sensors and Actuators A: Physical.* **207**, 39-42 (2014).
33. Meng, L. *et al.* Transportation of single cell and microbubbles by phase-shift introduced to standing leaky surface acoustic waves. *Biomicrofluidics.* **5** (4), 044104 (2011).
34. Sriphutkiat, Y., Zhou, Y. Particle manipulation using standing surface acoustic waves (SSAW) at dual frequency excitation: effect of power ratio. *Sensors and Actuators A: Physical.* **263**, 521-529 (2017).
35. Batchelor, G. K. *An Introduction to Fluid Dynamics.* Cambridge University Press. Cambridge, UK (2000).
36. Glynne-Jones, P., Hill, M. Acoustofluidics 23: acoustic manipulation combined with other force fields. *Lab on a Chip.* **13** (6), 1003-1010 (2013).
37. Winkler, A., Brünig, R., Faust, C., Weser, R., Schmidt, H. Towards efficient surface acoustic wave (SAW)-based microfluidic actuators. *Sensors and Actuators A: Physical.* **247**, 259-268 (2016).
38. Chen, Y. *et al.* Standing surface acoustic wave (SSAW)-based microfluidic cytometer. *Lab on a Chip.* **14**, 916-23 (2014).
39. Devendran, C. *et al.* The importance of travelling wave components in standing surface acoustic wave (SSAW) systems. *Lab on a Chip.* **16**, 3756-66 (2016).
40. Destgeer, G. *et al.* Submicron separation of microspheres via travelling surface acoustic waves. *Lab on a Chip.* **14**, 4665-72 (2014).
41. Ding, X. *et al.* Standing surface acoustic wave (SSAW) based multichannel cell sorting. *Lab on a Chip.* **12**, 4228-31 (2012).
42. Chen, Y. *et al.* Continuous enrichment of low-abundance cell samples using standing surface acoustic waves (SSAW). *Lab on a Chip.* **14**, 924-30 (2014).

